WILEY-VCH

An unusual plank-shaped nematogen with a graphene nanoribbon core

Giliandro Farias,[a] David da S. Simeão,[b] Thamires S. Moreira,[c] Paloma L. dos Santos,[d] Ahmed Bentaleb,[c] Andrew P. Monkman,[d] Juliana Eccher,[b] Fabien Durola,[c] Harald Bock,*[c] Bernardo de Souza,*[a] and Ivan H. Bechtold*[b]

Abstract: A [12]phenacene exclusively decorated with four lateral hexylester substituents self-assembles into a nematic liquid crystal glass on cooling after melting at high temperature. This uniaxial nematic organization of a plank-shaped nanographene is unprecedented and in strong contrast to the common design rules for liquid crystals. Highly birefringent samples can be obtained in homogeneously planar or twisted waveguiding configurations that are stable against crystallization at and below room temperature and up to 100°C.

Introduction

Nematics are the simplest and most abundant type of liquid crystals, and come in a great variety of molecular structures. To form a standard (uniaxial) nematic mesophase, i.e. a liquid with no long-range positional molecular order but with macroscopic anisotropic orientation along one preferred direction, one of two basic molecular shapes is generally required: Either the semi-flexible molecule is long in one dimension and short in the two others, i.e. a semi-flexible rod, or it is long in two dimensions and short in the third, i.e. a semi-flexible disk. Whilst rod-shaped nematogens are extremely abundant, disk-shaped ones are much rarer, because bidimensional disk-shaped molecules tend to aggregate more strongly than rods and thus prefer columnar mesophases with periodic positional order. The most common molecular structure of rod-shaped nematogens is a combination of two or more benzene units, linked either directly as in biphenyl, or via linker moieties such as –COO- or –N=CH-, plus one or two terminal flexible linear alkyl, alkoxy or alkylester substituents, that lengthen further the structure and add flexibility. Often also a polar head group, such as –CN, is present, increasing the polarizability

of the conjugated pi-electron system along the rod. The flexible alkyl substituents are almost always linked to the head or tail of the aromatic rod-shaped unit, and not laterally, because lateral substitution reduces the anisotropic molecular shape and quickly leads to the loss of the nematic behavior. Even if the aromatic part is extremely elongated, only very small lateral alkyl extensions are tolerated, and terminal alkyl groups should preferably be present as well to compensate the lateral extension. A particularly illustrating example is the family of terminally and laterally alkyl-substituted 1,4-bis[2-[4-(2-phenylethynyl)phenyl]ethynyl]-benzenes **1** described by Yatabe et al. [1] The alkyl substituents R1, R2 and R3 on its near-ideally rod-shaped, strongly nematogenic core have been varied systematically to study the destabilization of the nematic behavior by lateral alkyl substitution and its stabilization by terminal alkyl substitution. With R1=octyl, R2=hexyl and R3=H, i.e. with two long terminal and two long lateral chains, an enantiotropic nematic phase was observed, but if R3 is increased to ethyl, no mesophase was observed. The mesophase reappears if R2 is shortened to ethyl (i.e. with R1=octyl and R2=R3=ethyl), but even without R2, lengthening R3 just to propyl destroys the mesophase in spite of the presence of long terminal chains R1. With R1=R3=H and R2=octyl, i.e. with only two long lateral chains, no mesophase was observed either. Thus even in this family that has an extremely pronounced rod shape of the rigid part of the molecule, the nematic mesophase is very fragile towards the introduction of lateral alkyl chains.
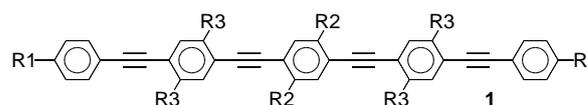
Scheme 1. Near-ideally rod-shaped phenylethinyl tetramers, whose nematic mesophase is easily suppressed by introducing lateral alkyl chains R2 and R3.[1]

If the conjugated rigid part of the molecule is itself extended in one lateral direction, one would expect increased stacking, favoring 3D crystalline, 2D columnar or 1D smectic (lamellar) periodicity at the expense of nematic (i.e. orientation-only) order. This strong tendency to stack via intermolecular dipolar or pi-electron interactions also has thwarted efforts to obtain the elusive biaxial nematic mesophase with rigid plank-shaped mesogens; this goal has instead been reached by less rigid lateral extensions using flexible macrocycles [2] or bow-shaped mesogens [3]. Extended semi-flexible molecular cores bearing more than two terminal chains (the so-called tetra- and hexacatenar mesogens) have

[a]   G. Farias, Prof. B. de Souza
      Departamento de Química, Universidade Federal de Santa Catarina
      88040-900 Florianópolis, SC, Brazil
      bernardo.souza@ufsc.br
[b]   D. da S. Simeão, Prof. J. Eccher, Prof. I. H. Bechtold
      Departamento de Física, Universidade Federal de Santa Catarina
      88040-900 Florianópolis, SC, Brazil
      ivan.bechtold@ufsc.br
[c]   T. S. Moreira, A. Bentaleb, Dr. F. Durola, Dr. H. Bock
      Centre de Recherche Paul Pascal, CNRS & Université de Bordeaux
      115, av. Schweitzer, 33600 Pessac, France
      bock@crpp-bordeaux.cnrs.fr
[d]   P. L. dos Santos, Prof. A. P. Monkman
      Department of Physics, Durham University, South Road, Durham,
      DH1 3LE, U.K.

      Supporting information for this article is given via a link at the end of
      the document.

also failed to give a biaxial nematic mesophase, but they give in some cases a standard (uniaxial) nematic mesophase [4].

Some of us recently developed the synthesis of long phenacenes decorated with four solubilizing lateral alkylester moieties [5], because phenacenes are the simplest fully condensed stable graphene ribbons (in contrast to the much less stable acenes) and thus are of fundamental interest as archetypal pi electron systems. All members of this family, i.e. tetraester derivatives **2-5** of [8]-, [10]-, [12]- and [14]phenacene, directly melt upon heating from the crystalline to the isotropic liquid state, without intermittent appearance of an enantiotropic liquid crystalline mesophase.
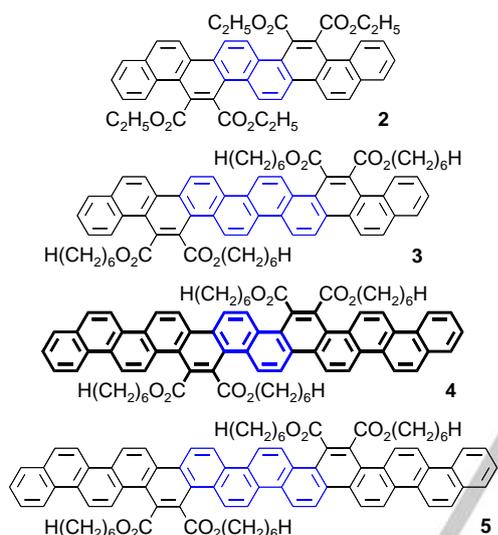
Scheme 2. Plank-shaped phenacenes with four lateral alkylester chains.[5] Central unsubstituted phenacene fragments are marked in blue. The nematic liquid crystalline homologue **4** is highlighted in bold.

Results and Discussion

We have now found that the [12]phenacene derivative **4** surprisingly shows a monotropic nematic phase when, after melting at 247°C [6], the isotropic liquid is cooled to 241°C. No nematic behavior could be observed with the shorter and longer homologues **2**, **3** and **5**.

Given that nematic phases of rod-shaped molecules with only lateral flexible substituents have to our knowledge never been observed before, the occurrence of such a phase in elongated plank-shaped **4** is intriguing, especially in the absence of any such phase in the more elongated **5**. Whilst the absence of a mesophase in the shortest homologue **2** may be attributed to its less anisotropic shape, one possible explanation for the absence of a mesophase in **5** and **3** is that contrary to **4**, both possess a rather long unsubstituted chrysene fragment in the middle, which allows easier intermolecular non-parallel stacking interactions than the shorter central naphthalene unit in **4**.
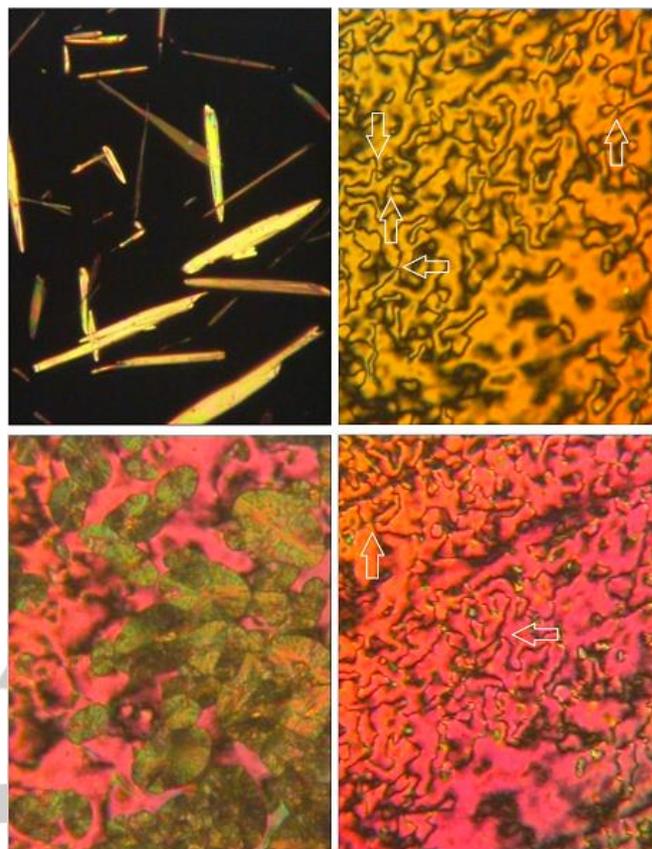
Figure 1. Microscopic textures of **4** between untreated glass plates (POM with crossed polarizers): Top left: Melting needle-shaped crystals at 247°C. Top right: Nematic Schlieren texture at 240°C showing four-brush defects (highlighted by arrows) characteristic of a nematic phase of uniaxial symmetry [7]. Bottom left: Nematic texture with spherulitic crystals growing in the bulk upon waiting at 160°C. Bottom right: Nematic Schlieren texture after fast cooling to room temperature, showing four-brush defects (highlighted by arrows).

Upon slow cooling or at constant elevated temperature, crystallization is observed (various crystalline textures can be observed depending on temperature). At temperatures above 170°C, this crystal growth nucleates slowly at the rim of the sample, i.e. at defects at its air interface, whilst below 170°C, crystallization starts from multiple nucleation sites in the bulk of the material. Upon fast cooling to temperatures around 100°C or below, the typical nematic Schlieren texture of **4** between glass plates is maintained down to ambient temperature (Figure 1). This suggests that a nematic glass is formed upon fast cooling below a critical temperature, allowing the conservation of nematic order at room temperature. To confirm this, we performed powder X-ray diffraction studies on a bulk sample in a glass capillary at different temperatures (Figure 2). Upon stepwise heating, with diffractograms recorded every 50 degrees, of a sample quickly cooled from 250 to 0°C, only a very broad peak at $q = 0.35$ Å^{-1} corresponding to an average intermolecular distance of *c.* 18 Å is observed at 0, 50 and 100°C, indicating the absence of any long-range periodicity, whereas crystalline order is manifest at 150 and 200°C. At 250°C, again only a diffuse peak at $q = 0.35$ Å^{-1} is

observed. Upon stepwise cooling from high temperature to 150°C, with diffractograms recorded every 10 degrees, only the diffuse peak is observed down to 170°C, whilst a multitude of peaks characteristic of crystalline order appear at lower temperature [Figure 2]. Albeit no significant difference can be discerned between the diffractograms in the isotropic phase at 250°C and those either at lower temperature before the onset of crystallization or at 0 to 100°C after fast cooling, the absence of any sharp peaks together with the corresponding textures observed by POM confirm conclusively the formation of a nematic phase upon cooling the isotropic liquid and the conservation of the nematic order at low temperature without any "texture-neutral" crystallization that might pass unobserved at POM.
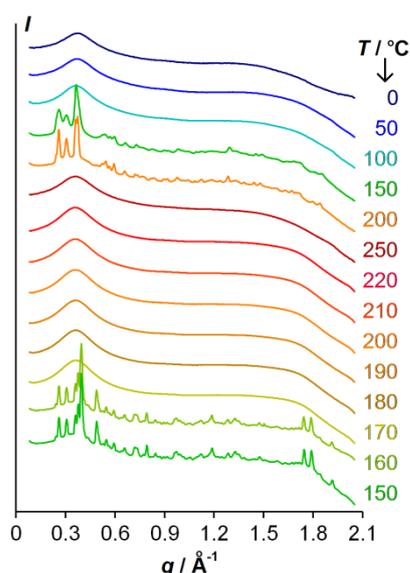
Figure 2. Evolution of the powder X-ray diffraction pattern of a bulk sample of **4** after fast cooling from 250 to 0°C. The sample is first reheated stepwise to 250°C and then cooled stepwise to 150°C (in chronological order from top to bottom, data acquisition time at each temperature: 1h).

As the molecular shape of **4** is moderately biaxial, due both to the flat ribbon shape of the arene core and to the presence of four lateral chains, and as the occurrence of a nematic phase in a lateral-chains-only rod or plank is unprecedented, the question arises whether the nematic mesophase is biaxial. Contrary to Schlieren textures of uniaxial nematics, that display both four- and two-brush defects, four-brush defects are symmetry-impeded in biaxial phases [7]. Albeit the number of four-brush defects is lower in the nematic glass at room temperature than in the fluid mesophase at high temperatures, four-brush defects are clearly present in both (Figure 1); the mesophase is thus uniaxial at all temperatures.

The highly delocalized pi electron system suggests a high birefringence Δn, even in the absence of polarizing terminal groups such as cyano (-CN) or isothiocyanato (-NCS), commonly employed in small molecule nematic liquid crystals. Indeed, upon cooling a 4µm ± 0.5µm thick cell from 250°C down to the onset of crystallization, the birefringence color runs through three color

cycles to reach the pale green-yellow beyond third-order red before crystallizing at 170°C, corresponding to a birefringence of $\Delta n = 0.45 \pm 0.1$ [8] a value typically obtained with nematic isothiocyanate mixtures optimized for high birefringence applications [9]. The extended and rigid, yet apolar conjugated pi electron system of **4** thus gives rise to a birefringence that reaches the values of highly polar materials designed for maximum birefringence.

To explore whether the direction of polarization can be homogeneously and macroscopically orientated, we needed an aligning anisotropic surface that is stable and maintains its anisotropy and aligning effect at temperatures close to 250°C, in the vicinity of the phase transition temperatures of **4** where annealing is most efficient. Particularly temperature-resistant aligning surfaces are known to result from rubbing teflon onto heated glass substrates [10,11]. We confirmed that teflon-coated glass plates obtained by rubbing a teflon bar on glass substrates heated to 150°C maintain their microgroove surface structure upon annealing at 260°C (see supporting information, S1). Compound **4** was sandwiched between two teflon-coated glass plates with parallel rubbing directions. After heating the sample to the isotropic liquid at 250°C and then cooling into the nematic phase at 240°C, a homogeneous planar texture was obtained. This uniform alignment could be preserved on fast cooling to room temperature, yielding uniformly oriented birefringent glassy nematic films, whereas slow cooling led to spherulitic crystallization (Figure 3a-c). A 90° twisted glassy nematic waveguiding film could be produced with similar ease when a sample between teflon-coated glass plates with perpendicular rubbing directions was cooled quickly from 250°C to room temperature (Figure 3d-f). These films confirm that the homogeneous director orientation of highly birefringent **4** can be frozen in unidirectional or helical geometries in its nematic glass state.
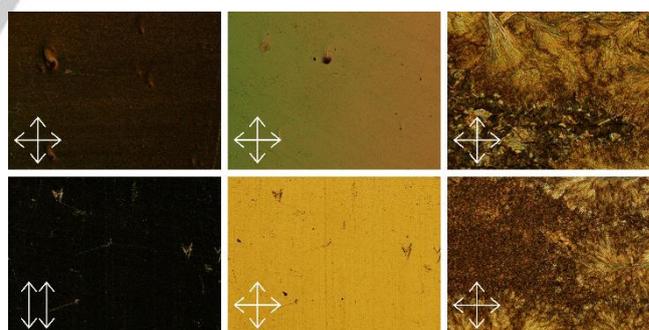
Figure 3. Microscopic textures of **4** between teflon-coated surfaces (POM) after fast (left and center) or slow (right) cooling from 250°C to room temperature. The arrows indicate polarizer and analyzer orientations. Top left: rubbing directions parallel to one polarizer; top center and right: rubbing directions oblique to both polarizers; bottom left, center and right: rubbing directions perpendicular to each other.

To assess the effect of homogeneous anisotropic orientation on the fluorescence emission, we compared the emission spectra of low concentration solution, spin-coated film and homogeneously

teflon-aligned nematic glass (Figure 4). Whereas the absorption maxima in solution (334 and 347 nm) and in the spin-coated film (337 nm) are very similar, their emission show different features. In solution, = the emission peak is at 451 nm while in solid state a much broader two-peaked emission spectra are observed , with peak positions at 479 and 544 nm in the spin-coated film, and 475 and 550 nm in the nematic glass). The absorption and emission broadening in film and nematic glass compared to the low concentration solution, together with the red shift of the emission spectra, testifies the stronger intermolecular interactions in solid state [12]. The pronounced dominance of the longer-wavelength peak in the nematic glass contrasts with a slight prevalence of the shorter-wavelength peak in the film. This evolution from a unique shorter-wavelength peak in solution via two near-equally intense peaks in film to a pronounced dominance of the longer-wavelength emission in the nematic glass strongly suggests that intermolecular aggregation with close chromophore contacts is most pronounced in the nematic glassy state with its supposed parallel alignment of chromophores.

Absorption and emission in solution as a function of concentration was performed to investigate the origin of the dominant peak around 550 nm for the nematic glass (Figure S2). The appearance of a new absorption shoulder around 425 nm for concentrations higher than 5×10^{-3} mol L^{-1} demonstrates that ground state dimers are formed. For concentrations close to 10^{-2} mol.L^{-1} the peak around 550 nm is already visible, becoming dominant for concentrations close to 10^{-1} mol.L^{-1}, and the shorter-wavelength peak at 475 nm is red-shifted if compared to the diluted solutions. The appearance of a new fluorescence band at much higher wavelength compared to the monomeric one in diluted solution, which increases with concentration and does not show vibronic structure, agrees with dimer origin.
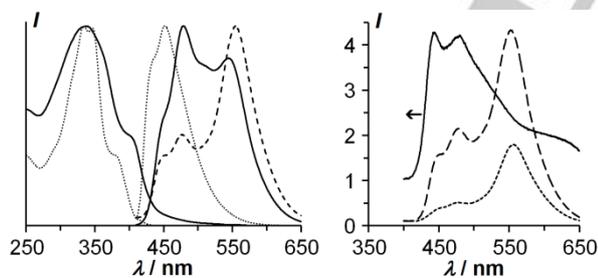
Figure 4. Left: Normalized absorption and emission spectra of **4** in chloroform solution (dotted) and spin-coated solid film (continuous), and emission in planar Teflon-aligned nematic glass (dashed). Emission spectra upon excitation at 347 nm (solution) or 335 nm (solid film and nematic glass). Right: Polarized emission spectra (arbitrary units) of planar aligned glassy nematic sample parallel (long dashes) and perpendicular (short dashes) to the alignment direction, and their dichroic ratio (continuous).

The lifetime τ of the excited state of **4** was measured on the planar aligned nematic glass to probe the emitting species separately at 475 nm and 550 nm. The fluorescence decay curves could be satisfactory fitted only with bi-exponentials, with the main (>90% contribution) component having a lifetime τ_1 of 1.3 ns at 475 nm and of 3.6 ns at 550 nm, which indicates different emitting species

(Table 1 and experimental curves in the supporting information, S3). Excimer formation is in most cases driven by the covalent interaction between excited π–π stacked molecules, and emission lifetimes of excimers are usually longer than those of monomeric states [13, 14]. We thus conclude that the fluorescence of the nematic glass has a contribution of monomeric states at 477 nm and aggregate states (dimer and excimer) with emission centered at 550 nm.

Table 1. Excited state lifetimes (τ) obtained from bi-exponential fittings of the fluorescence decay curves, their relative amplitudes (A), and fitting factors (χ^2) upon excitation at 475 and 550 nm.

λ / nm	τ_1 / ns	A_1 / %	τ_2 / ns	A_2 / %	χ^2
475	1.3 ± 0.1	95	6.0 ± 0.1	5	0.998
550	3.6 ± 0.2	92	11.3 ± 0.2	8	0.999

Surprisingly, the emission from the planar aligned nematic glass is much more strongly polarized at shorter than at longer wavelengths, with the dichroic ratio (between emission polarized parallel and perpendicular to the alignment direction) being 4.2:1 at 477 nm, and dropping to about 2.4:1 at the long-wavelength peak at 550 nm (Figure 4). The lateral aggregation manifested by the longer-wavelength peak leads to a less uniaxial character of the excited (emitting) state compared to the emission from strongly elongated and uniformly aligned individual chromophores at shorter wavelength.

The theoretical modeling of the isolated molecules **2-5** and its dimers yields the same pattern for the observed photophysical properties. By using TD-DFT, we computed the anisotropy of the transition dipole moment from the ground to the first excited state, which is related to the emission spectra and the birefringence. The predicted vertical energy difference between S_0 and S_1 for the isolated molecules and for their dimeric aggregates are coherent with what was observed, with the aggregates having smaller energy differences (Table S1). The anisotropy of the transition dipole moment, here measured as the ratio of its z and y components (along the ribbon axis and perpendicular to the aromatic plane, respectively), is accordingly much higher for the monomers than for the dimers, and has a strong polarization on the z axis along the aromatic scaffold (Figure S4 has a complete definition of the axes). This is consistent with the observed large birefringence and dichroic ratio.

Figure 5 shows the difference in densities between the S_0 and S_1 states of **4**, with the long chains substituted by a methyl, and its dimer (see Figure S5-S6 for all molecules). During the electronic excitation (or deexcitation in fluorescence), there is a large electron density shift along the z axis for the monomer. That is somewhat reduced in the dimer, because parts of the density also go along the y direction, perpendicular to the aromatic rings and into the neighboring molecule. That diminishes the magnitude of the transition dipole vector and correlates directly with the lower emission rate and longer lifetime observed [15,16].
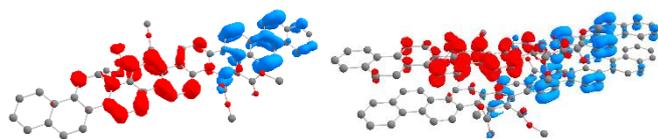
Figure 5. Difference in electronic density between the S_0 and S_1 states for a model of molecule **4** and its dimer, calculated using BP86/DEF2-TZVP. The blue represents a depletion while the red an increase in electronic density. Hydrogens are omitted for clarity.

It appears thus that from the properties of the isolated molecules alone, a reason for **4** being the only material presenting a mesophase cannot satisfactorily be inferred. Whilst the simulations of **2**, with a more isotropic pattern of electron density shifts upon excitation (at least to the S_1), may explain its disproportionately low polarizability compared to **3-5**, the electric properties (dipole moment, quadrupole moment and polarizability) of these three longer homologs grow as expected with length and start to saturate at some point, without anything specific to **4** (Figure S7-S9 and Table S2-S4).

This suggests that the propensity to mesophase formation is attributable to a complex combination of short- and medium-range intermolecular interactions in the bulk and thus a more complex model would be necessary to understand it.

Conclusions

In summary, extended twelve-ring graphene nanoribbon segments that are appropriately decorated with solubilizing lateral chains self-assemble in parallel to form a strongly anisotropic nematic glass. This amplification of molecular anisotropy into an orientable bulk fluid anisotropic structure, whilst being a trivial feature of liquid crystals, is highly unexpected for graphene nanoribbon segments given their strong tendency to aggregate in positionally ordered π-stacked structures. Uniform macroscopic anisotropic alignment is conveniently obtained in twisted and straight configurations at ambient temperatures, showing high birefringence as well as polarized fluorescence as manifestations of strong anisotropic polarizability, a key prerequisite for graphene nanoribbon optoelectronics.

Experimental Section

Spin-coated films of 125 nm thickness with a mean surface roughness of less than 2.0 nm were produced by spinning a solution of 10 mg/mL in chloroform at 1500 rpm for 30 s. The thickness and roughness of the spin-coated films were determined with a Nanosurf Flex AFM, operating in tapping mode under ambient conditions with a scanning rate of 1.0 Hz and 512×512 pixels. Excited state lifetimes were measured at room temperature in air with a DeltaFlex TCSPC system from Horiba using LED excitation at 357 nm and emission collection at 475 nm and 550 nm.

[1] T. Yatabe, Y. Suzuki, Y. Kawanishi, *J. Mater. Chem.* **2008**, *18*, 4468-4477.

[2] J.-F. Li, V. Percec, C. Rosenblatt, O. D. Lavrentovich, *Europhys. Lett.* **1994**, *25*, 199-204.

[3] a) M. Lehmann, S.-W. Kang, C. Köhn, S. Haseloh, U. Kolb, D. Schollmeyer, Q. B. Wang S. Kumar, *J. Mater. Chem.* **2006**, *16*, 4326-4334; b) M. Lehmann, C. Köhn, J. L. Figueirinhas, G. Feio, C. Cruz, R. Y. Dong, *Chem. Eur. J.* **2010**, *16*, 8275-8279; c) J. Seltmann, K. Müller, S. Klein, M. Lehmann, Chem. Commun. **2011**, *47*, 6680-6682.

[4] M. Gharbia, A. Gharbi, H. T. Nguyen, J. Malthête, *Curr. Opin. Colloid Interface Sci.* **2002**, *7*, 312-325.

[5] T. S. Moreira, M. Ferreira, A. Dall'armellina, R. Cristiano, H. Gallardo, E. A. Hillard, H. Bock, F. Durola, *Eur. J. Org. Chem.* **2017**, 4548-4551.

[6] The polymorphic microcrystalline material, obtained after repeated column chromatography in dichloromethane on silica followed by repeated crystallization from butanol, partially melts at 242°C, as observed by polarized light optical microscopy (POM), to give way to a mixture of slowly growing crystalline needles surrounded by isotropic liquid. These needles melt upon further heating at 247°C.

[7] S. Chandrasekhar, G. G. Nair, K. Praefcke, D. Singer, *Mol. Cryst. Liq. Cryst.* **1996**, *288*, 7-14.

[8] F. D. Bloss, *An Introduction to the Methods of Optical Crystallography*, Saunders College Publishing 1961, ISBN 0-03-010220-0.

[9] S. Gauza, J. Li, S.-T. Wu, A. Spadło, R. Dabrowski, Y.-N. Tzeng, K.-L. Cheng, *Liq. Cryst.* **2005**, *32*, 1077-1085.

[10] J. C. Wittmann, P. Smith, *Nature* **1991**, *352*, 414-417.

[11] I.H. Bechtold, E.A. Oliveira, Mol. Cryst. Liq. Cryst., Vol. 442, pp. 41–49, 2005.

[12] P. Apostol, J. Eccher, M.E.R. Dotto, C.B. Costa, T. Cazati, E.A. Hillard, H. Bock, I.H. Bechtold, *Phys.Chem.Chem.Phys.*, **2015**, 17, 32390-32397.

[13] E.A. Margulies, L.E. Shoer, S.W. Eaton, M.R. Wasielewski, Phys. Chem. Chem. Phys. 16 (2014) 23735–23742.

[14] J. Eccher, A.C.B. Almeida, T. Cazati, H. von Seggern, H. Bock, I.H. Bechtold, *Journal of Luminescence* **2016**, *180*, 31-37.

[15] N.J. Turro, J.C. Scaiano, V. Ramamurthy, *Modern Molecular Photochemistry of Organic Molecules*, University Science Books, 2010, ISBN 978-1891389252.

[16] B. de Souza, F. Neese, R. Izsák, *J. Chem. Phys.*, 148, 034104, **2018**.

Entry for the Table of Contents (Please choose one layout)

Layout 1:

FULL PAPER or COMMUNICATION

Laterally decorated ribbon-shaped graphene segments made of twelve benzene units self-assemble into a nematic anisotropic glass at room temperature with high birefringence and polarized fluorescence.
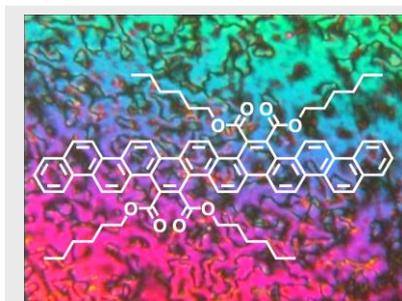
Author(s), Corresponding Author(s)*

Page No. – Page No.

An unusual plank-shaped nematogen with a graphene nanoribbon core

Layout 2:

FULL PAPER or COMMUNICATION

((Insert TOC Graphic here; max. width: 11.5 cm; max. height: 2.5 cm))

Author(s), Corresponding Author(s)*

Page No. – Page No.

Title

Text for Table of Contents